The Journal of Neuroscience, December 1995, 15(12): 8011–8022

Two Voltage-Dependent K^+ Conductances with Complementary Functions in Postsynaptic Integration at a Central Auditory Synapse

Helen M. Brew and Ian D. Forsythe

Ion Channel Group, Department of Cell Physiology and Pharmacology, University of Leicester, Leicester LE1 9HN, United Kingdom

The medial nucleus of the trapezoid body (MNTB) relays auditory information important for sound source localization. MNTB neurons faithfully preserve the temporal patterning of action potentials (APs) occurring in their single giant input synapse, even at high frequencies. The aim of this work was to examine the postsynaptic potassium conductances that shape the transfer of auditory information across this glutamatergic synapse. We used whole cell patch techniques to record from MNTB neurons in thin slices of rat brainstem. Two types of potassium conductance were found which had a strong influence on an MNTB neuron's postsynaptic response. A small low voltage threshold current, I_d, limited the response during each EPSP to a single brief AP. I_d was specifically blocked by dendrotoxin (DTX), resulting in additional APs during the tail end of the EPSP. Thus DTX degraded the temporal fidelity of synaptic transmission, since one presynaptic AP then led to several postsynaptic APs. A second conductance was a fast delayed rectifier with a high voltage activation threshold, that rapidly repolarised APs and thus facilitated high frequency AP responses. Together, these two conductances allow high frequency auditory information to be passed accurately across the MNTB relay synapse and separately, such conductances may perform analogous functions elsewhere in the nervous system.

[Key words: medial nucleus of the trapezoid body (MNTB), potassium channels, dendrotoxin, synaptic transmission, giant synapse, EPSP, temporal fidelity, action potential frequency, action potential duration, brainstem slices, sound localization, auditory system]

The medial nucleus of the trapezoid body (MNTB) forms a specialized relay in brainstem auditory pathways involved in sound source localization (Fig. 1*A*). Contralateral auditory signals are relayed across the single giant glutamatergic synapse, or calyx of Held, which enfolds the soma of each MNTB principal neuron (Held, 1893; Banks and Smith, 1992; Forsythe, 1994). Each calyx arises from a globular bushy neuron (GBN) located in the contralateral cochlear nucleus (CN) (Tolbert et al., 1982). The MNTB neurons form glycinergic inhibitory synapses onto neurons of the lateral superior olive (LSO) (Moore and Caspary, 1983; Wenthold et al., 1987). LSO neurons encode the relative amplitude of sounds at each ear, by comparing these contralateral inhibitory inputs with the excitatory inputs that they receive directly from bushy neurons of the ipsilateral CN (Fig. 1*A*). Relative binaural amplitude is thought to be an important indicator of the azimuthal location of a sound source, and therefore crucial to sound source localization (reviewed by Masterton and Imig, 1984). The temporal patterning of action potentials (APs) is accurately preserved across the GBN-MNTB synapse, at frequencies as high as 600 Hz (Wu and Kelly, 1993). This suggests that precise timing cues, including phase-locked APs, may be used by LSO neurons to aid their encoding of relative binaural amplitude, thus helping the nervous system to localize and discriminate between sound sources.

Rapidly desensitizing AMPA-type glutamate receptors underly the large, rapidly decaying excitatory postsynaptic potentials (EPSPs) generated by giant calyceal synapses onto MNTB neurons (Forsythe and Barnes-Davies, 1993b) and other auditory neurons (Raman et al., 1994; Zhang and Trussell, 1994b). The large rapidly decaying EPSP causes the rapid and secure generation of a single AP in both MNTB neurons (Banks and Smith, 1992; Forsythe and Barnes-Davies, 1993b) and in the avian equivalent of GBNs (Zhang and Trussell, 1994a) thus contributing to the high reliability and temporal fidelity of synaptic transmission in these auditory pathways. Sustained depolarizing current steps cause a similar characteristic response, a single initial AP, suggesting that intrinsic membrane currents prevent any subsequent APs in MNTB neurons (Forsythe and Barnes-Davies, 1993a) and other auditory neurons (see Discussion). In the presence of the potassium channel blocker 4-aminopyridine (4-AP) depolarizing steps cause multiple, broadened APs, and some of the membrane conductance is blocked (shown for MNTB neurons by Banks and Smith, 1992; Forsythe and Barnes-Davies, 1993a) suggesting that one or more 4-AP-sensitive conductances limit AP firing and could therefore contribute to synaptic fidelity.

We have exploited the relative simplicity of the GBN-MNTB synapse to analyze MNTB neuron potassium conductances in more detail and investigate their role in shaping AP responses to synaptic activation, including the maintenance of high frequency synaptic fidelity. The properties of these conductances correlate with those of channels formed by potassium channel

Received May 16, 1995; revised Aug. 3, 1995; accepted Aug. 8, 1995.

Thanks to Margaret Barnes-Davies, Jennifer Albert, and David Attwell for reading and criticizing the manuscript, and to Dr. Brian Robertson of Wyeth Laboratories UK for the gift of Toxin-I. Thanks also to Diane Everitt and William King for technical assistance. Supported by the Wellcome Trust. I.D.F. is a Wellcome Senior Research Fellow in Basic Biomedical Sciences.

Correspondence should be addressed to Dr. H. M. Brew at Ion Channel Group, Department of Cell Physiology and Pharmacology, University of Leicester, P.O. Box 138, Leicester LE1 9HN, United Kingdom.

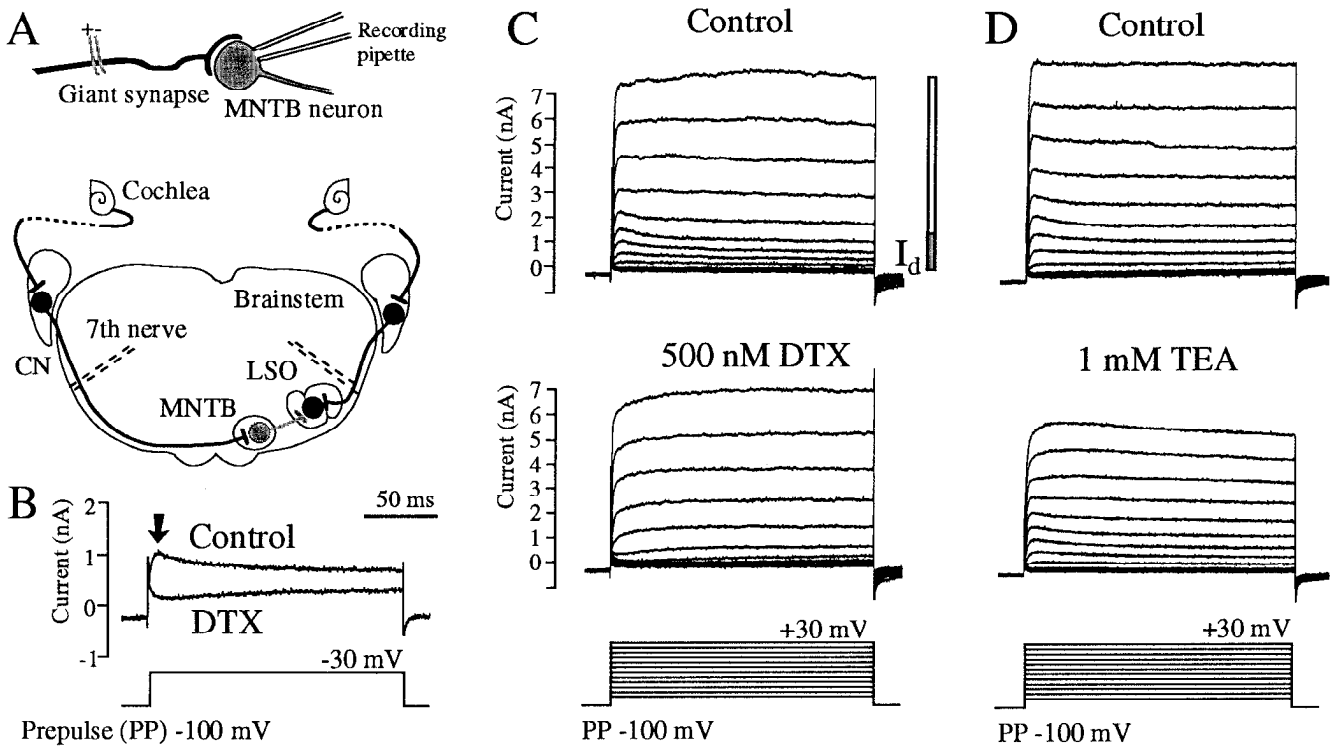

Figure 1. DTX and TEA block different components of the outward current in voltage-clamped MNTB neurons. *A*, The upper diagram shows the giant synapse on the MNTB neuron soma, the location of the recording pipette and the electrodes used for presynaptic stimulation. The lower diagram is a transverse section of the rat brainstem, based on the appearance of the experimental slices, showing the wiring that underlies relative binaural loudness encoding by neurons in the lateral superior olive (*LSO*). The cochlear nucleus (*CN*) and MNTB are also shown. All synapses are excitatory (glutamatergic, shown in *black*) except the MNTB neuron inhibitory output synapses (glycinergic, in *gray*). *B*, The control outward current in an MNTB neuron at −30 mV peaked after about 5 msec (*arrow*) then slowly inactivated, in control ACSF-V (expanded traces from *C*); 500 nM DTX blocked most of this outward current. *C*, The outward currents from the same MNTB neuron as in *B*, stepped to potentials between −80 mV and +30 mV for 180 msec, after a 750 msec prepulse potential of −100 mV, in control ACSF-V (upper current set). An early-peaking low threshold current component, I_d, was the predominant current in the potential range roughly indicated by the *shaded bar*. In the presence of 500 nM DTX there was no remaining outward current at potentials negative to −30 mV (lower set of currents). *D*, Another MNTB neuron displays the same low threshold current component; 1 mM TEA blocked some current at more positive potentials, but spared the low threshold component.

subunits known to be present in MNTB neurons, giving insights into the probable functions of similar channels elsewhere in the nervous system.

Preliminary abstracts of parts of this work are published in Brew and Forsythe (1994a,b).

Materials and Methods

Preparation and incubation of brainstem slices. Thin brain slices were obtained as in Edwards et al. (1989) with minor modifications. The brain was removed from recently decapitated 5–15 d old Lister hooded rats and placed in an ice-cold bicarbonate-buffered solution gassed with 95% O_2, 5% CO_2 mixture. (This solution used for dissection and slicing was similar to the standard artificial cerebrospinal fluid, ACSF, described below, but with the sodium chloride replaced by iso-osmotic sucrose.) The brainstem was glued to a vibratome stage (Lancer Series 1000, Technical Products International, St. Louis, MO) while five or six transverse slices (200 μm thick) were cut from the part of the brainstem containing the MNTB (Fig. 1*A*). Slices were incubated for 1 hr at 37°C in gassed standard ACSF (pH 7.4) containing (in mM): NaCl 125, KCl 2.5, $NaHCO_3$ 26, NaH_2PO_4 1.25, Na pyruvate 2, myo-inositol 3, glucose 10, $CaCl_2$ 2, $MgCl_2$ 1. After incubation, slices remained in gassed ACSF, but were kept at room temperature. These procedures are described in more detail elsewhere (Forsythe et al., 1995).

Electrophysiological recordings. For recording, a slice was placed in a Peltier-driven environmental chamber mounted on a microscope (model M2A, Microinstruments, Oxford, UK) fitted with Nomarski optics and a 40× (NA 0.55) water immersion objective (Nikon). The chamber was continually perfused (1 ml/min, 25°C) with gassed standard ACSF, termed ACSF-C because of its use in current-clamp experiments. An alternative low calcium ACSF-V was used during voltage-clamp studies of intrinsic whole cell currents, designed to block sodium channels, minimise calcium currents and reduce synaptic activity. The ACSF-V contained (in mM): $CaCl_2$ 0.5, $MgCl_2$ 2.5, strychnine 0.01, tetrodotoxin 0.001 (other contents as for the standard ACSF-C). During the synaptic stimulation experiments ACSF-C was used for both voltage-clamp and current-clamp recordings. Other drugs were applied by perfusion in the relevant ACSF. Drugs were obtained from Sigma-Aldrich (Poole, UK) except tetrodotoxin (Calbiochem-Novabiochem, Nottingham, UK) and DTX (Toxin-I, purified from the venom of *Dendroaspis polylepis polylepis*) which was a gift from Brian Robertson of Wyeth Laboratories (Taplow, Maidenhead, UK).

Recordings were made from visually identified MNTB neurons using the whole cell configuration of the patch-clamp technique. Patch pipettes were drawn from thin-walled borosilicate glass (Clark Electromedical Instruments, Reading, UK) and filled with a solution that contained (in mM): Kgluconate 97.5, KCl 32.5, EGTA 5, HEPES 10, $MgCl_2$ 1 (pH 7.2). These pipettes had a resistance of 3–5 MΩ when immersed in ACSF-C in the recording chamber. The patch-clamp amplifier was an Axopatch 200A (Axon Instruments, Foster City, CA). During whole cell recordings, the series resistance between the cell interior and the pipette was frequently monitored and kept as stable as possible. The mean cell capacitance in 42 MNTB neurons was 19.8 (±0.9) pF with a mean series resistance of 10.2 (±0.5) MΩ (rising to 13.6 MΩ by the end of the recording). The Axopatch "prediction" circuitry was always set to 85%, reducing the mean time constant for voltage clamping the neuronal membrane from 0.2 msec to 0.03 msec. The Axopatch "correction" circuitry was also set to 85%, reducing the voltage errors due to, for example, 5 nA current flow across the series resistance from an average of 51 mV down to 7.7 mV, and reducing current filtering from 500 Hz to about 4 kHz.

As usual for whole cell recordings in slices, the axon and dendrites can only be voltage clamped effectively close to the recording site, the MNTB neuron soma. However, the sparse dendrites of MNTB neurons probably meant there was less filtering of the recorded currents than usual for neuronal recordings from other preparations. Also current kinetics, and AP firing frequencies were slower at 25°C than they would be *in vivo*. The large currents in MNTB neurons sometimes restricted the range of voltage steps that could be used (the amplifier could not supply more than 10 nA) or resulted in voltage drops at the pipette tip. At very positive potentials, open potassium channels reduced membrane resistance to values comparable with the series resistance, therefore reducing the membrane time constant below the value set within the compensation circuitry. Thus, the voltage clamp is likely to be of lower quality immediately after a return to more negative potentials and some currents could be generated by the temporarily mismatched compensation circuitry as well as by voltage-dependent conductances. These restrictions do not affect the main conclusions of this article, which emphasise qualitative distinctions between the conductance types.

The voltage values shown in this article are the pipette voltages rather than estimates of the true membrane potential after correction for any remaining uncompensated series resistance (see above). The voltage values also exclude the junction potential of −7 mV (unless otherwise stated) thus representing pipette command voltages and pipette resting potentials. No leak current was subtracted from any of the raw current traces (shown in Figs. 1, 3, 4).

For the synaptic stimulation experiments, a bipolar stimulating electrode was positioned near the midline of the trapezoid body (Forsythe et al., 1995) to stimulate the axon giving rise to the giant synapse onto the MNTB neuron soma (top part of Fig. 1*A*).

Data acquisition and analysis. Data was acquired via a 1401plus interface using PATCH AND VOLTAGE CLAMP software (Cambridge Electronic Design Ltd., Cambridge, UK) running on a 486 computer. Data was filtered at 2 kHz and digitized at 5 kHz (or, for some AP recordings, filtered at 5 kHz and digitized at 10 kHz). The same software was also used for most of the data analysis. Current amplitudes were the average of five data points around the measurement time, usually 5 msec after the start of voltage steps. Tail currents were fitted with single or double exponential decay functions between 1.2 msec and 50 msec after the end of the main current step. The fitting used a least-squares iterative method, with starting values for fit parameters supplied by the user. Averaged data for several neurons is expressed as mean ± the standard error of the mean, followed by the number of neurons.

Some further analysis of current–voltage relations, including activation and inactivation curves, was performed within a spreadsheet on a Macintosh computer. If recordings included significant leak currents, they were subtracted using current values from pipette potentials between −100 mV and −60 mV to estimate the leak magnitude. The activation and inactivation plots of the dependence of conductance, G, on voltage, V, were fitted using a Boltzmann equation of the form

$$G = G_{max}/(1 + e^{(V-V_{half})/K}),$$

with variables G_{max}, V_{half} and K (the slope factor). For the inactivation curves, an additional variable, G_{min}, was used in the Boltzmann equation, to fit the minimum as well as maximum current values.

Results

A low voltage threshold DTX-sensitive potassium conductance in MNTB neurons

One potassium conductance type in whole-cell voltage-clamped MNTB neurons was selectively and irreversibly blocked by Toxin-I, a dendrotoxin (DTX) from black mamba snake venom (Strydom, 1976) which is homologous to dendrotoxins from green mamba venom (Harvey and Karlsson, 1982). Data from some recordings (fewer than 10%) where this low threshold current was absent or very small were excluded from the analysis. Data presented in this paper is from 61 different MNTB neurons. The characteristic outward potassium currents seen in the control artificial cerebrospinal fluid (ACSF-V, for voltage-clamp experiments) included a low voltage threshold component that activated rapidly at −30 mV, peaking 5 msec after the start of a voltage step, then showing some slow inactivation (Fig. 1*B–D*, control currents). The outward current showed slower activation at −50 mV (Fig. 1*C,D*, control currents). The application of 500 nM DTX blocked most of the early outward current at −30 mV (Fig. 1*B*). DTX blocked this low voltage threshold component whereas the currents that began to activate at more positive potentials were unaffected (Fig. 1*C*); 1 mM tetraethylammonium (TEA) had little effect on this low threshold current component (Fig. 1*D*). A similar rapidly activating, slowly inactivating potassium current was first described in neurons of the rat nodose ganglion and termed I_d because of its sensitivity to α-dendrotoxin (Stansfeld et al., 1986).

The rapidly activating DTX-sensitive low threshold current, I_d, in MNTB neurons was very small compared to the outward currents seen at more positive potentials, which often reached 10 nA or more at +30 mV. For example, at −40 mV, the mean magnitude of the I_d current blocked by 100 nM DTX was 0.36 ± 0.06 nA (n = 9, currents measured 5 or 10 msec after the start of the step). At −50 mV or −40 mV, DTX reduced the current at 5 msec almost to the level of the leak current, which suggested that I_d was the predominant current at −40 mV (Fig. 2*A,C*, pooled data from 100 or 500 nM DTX). The proportion of the total current blocked at −40 mV was similar for three different DTX concentrations. At −40 mV, 100 nM DTX reduced the current by 82 ± 4% (n = 9) (measured 5 or 10 msec after the start of the step, and excluding leak current). 500 nM DTX reduced the current by a similar amount, 70% (n = 4), as did 10 nM DTX, 73% (n = 1) suggesting a K_d for DTX block below 10 nM. (The slowly activating DTX-insensitive current at −30 mV, shown in Fig. 1*B*, probably also accounted for the 20 to 30 % of current that was not blocked at −40 mV.)

At −30 mV, some inactivation of I_d occurred during 180 msec (e.g., Fig. 1*B*, control) though during much longer pulses inactivation remained incomplete (see Results below). The low voltage threshold current was mostly inactivated after one second at −30 mV, since the outward currents during voltage steps following a −30 mV prepulse were very similar to those of the currents in DTX following a −100 mV prepulse (Fig. 2*B*). In support of this, there was little effect of DTX on the mean currents (or their time courses of activation, data not shown) after a −30 mV prepulse lasting one second (Fig. 2*B*).

I_d activated rapidly over a more negative range of voltages than is typical for voltage-dependent potassium channels. The mean DTX-sensitive conductance was calculated and fitted with a Boltzmann curve (Fig. 2*F*). This gave an estimate of the voltage at which half the conductance was activated (V_{half}) as −42.7 mV, with a K value of 7.1 mV. The V_{half} for activation is therefore −50 mV after including the junction potential. (The true V_{half} for activation may be still more negative, because steps to potentials below −40 mV did not bring I_d channels to their equilibrium open level within 5 msec, the time at which the raw currents were measured.) This suggests that a small proportion of I_d channels could be open at −70 mV, if they were not inactivated, and could contribute to the MNTB neuron resting conductance.

A high threshold TEA-sensitive conductance does not inactivate at −30 mV

MNTB neurons also possessed a second potassium conductance with a higher voltage threshold, which was sensitive to a low concentration of the potassium channel blocker tetraethylammonium (TEA) as shown in Figure 1*D*. The effect of 1 mM TEA on the mean *I–V* relations from 6 MNTB neurons is shown in Figure 2*D*; 3 mM TEA blocked little more of the outward current

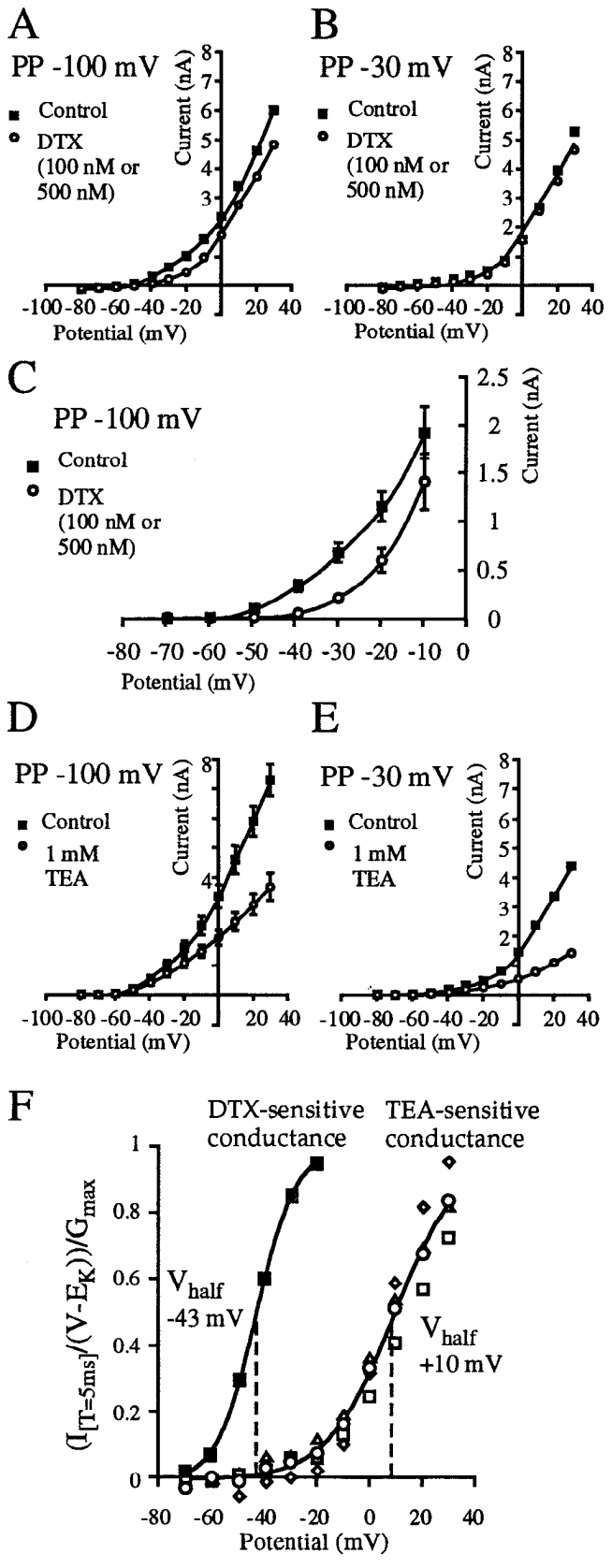

Figure 2. The effects of DTX and TEA on MNTB neuron current–voltage relations. Outward currents 5 msec after the start of each voltage step, after 750 msec prepulses of −100 mV (*A, C, D*) or −30 mV (*B, E*) were averaged from several neurons. Lines through the points were drawn by eye (except in *B* and *F*). *A*, The effect of 100 nM or 500 nM DTX on mean *I–V* relations from 5 MNTB neurons. *B*, The effect of DTX on the same neurons as in A, after an inactivating prepulse of −30 mV. The −30 mV prepulse removed (inactivated) a current component similar to the DTX-sensitive component, and DTX produced little further effect. The line through the points is the same line that goes through the DTX values of *A*. *C*, As in *A*, but at a larger scale, and using mean currents from 10 MNTB neurons; 500 or 100 nM DTX were applied (four and six neurons, respectively). The bars show SEs (except if smaller than the symbols). *D*, The effect of 1 mM TEA on mean *I–V* relations from 6 MNTB neurons. The bars show SEs. *E*, The effect of TEA on the same neurons as in *D*, after an inactivating prepulse of −30 mV. *F*, The voltage dependence of activation of I_d (*solid squares*) and the TEA-sensitive conductance (*open symbols*). The mean DTX-sensitive conductance at each voltage was estimated from the mean DTX-sensitive currents of the neurons in *A*, assuming an E_K of −80 mV. The curve was fitted using a Boltzmann equation (see Materials and Methods). The maximum conductance value given by the fitting procedure was used to normalize the plot. Activation curves for the TEA-sensitive conductance were calculated individually for four MNTB neurons (prepulses −30 mV). The TEA-sensitive conductance from one MNTB neuron (*open circles*) gave the example Boltzmann curve shown.

than 1 mM TEA. For example, at 0 mV, 3 mM TEA blocked 54.7 ± 4.4% of current (n = 4, data not shown) and 1 mM TEA blocked 41.9 + 4.3% (n = 6). This is consistent with a conductance having a K_d for TEA block of less than 1 mM.

One millimolar TEA blocked currents of similar magnitude and voltage dependence after a 1 sec −30 mV prepulse, as after a −100 mV prepulse (Fig. 2*D,E*). This suggests that the conductance blocked by TEA exhibits little inactivation at −30 mV (contrasting with I_d which was mostly inactivated by 1 sec at −30mV).

The TEA-sensitive conductance activated at much more positive potentials than I_d (Fig. 2*F*). The average V_{half} for activation was +10 mV, with a mean K value of 12.4 mV. Alternatively, activation curves could be calculated from the magnitude of the fast component of the current tails at −30 mV (see Fig. 3 and section below). This gave a mean V_{half} from three MNTB neurons of +1 mV, and a mean K of 10 mV (data not shown). The overall average V_{half} for activation was +5 mV, or −2 mV after including the junction potential.

The TEA-sensitive potassium channels open and close rapidly

The properties of a rapidly decaying component of tail currents in MNTB neurons suggest that it represents closing of the high threshold TEA-sensitive conductance. The tail currents at −30 mV following steps positive to −10 mV could be fitted using a double exponential decay (Fig. 3*A,B*, control tails). The fast tail component decayed with a mean time constant of 2.0 ± 0.3 msec (n = 11, after a step to +30 mV), was blocked by 3 mM TEA (Fig. 3*A*) and was insensitive to 100 nM DTX (Fig. 3*B*); 1 mM TEA blocked over 90% of this fast tail component (data not shown). The fast tail currents were still outward at −60 mV (supporting the idea that they reflect the closing of a potassium conductance) and decayed with a mean time constant of 1.3 ± 0.1 msec (n = 8, after +10 mV step). The fast tail currents were of the same magnitude after a −100 mV prepulse (Fig. 3*A*, control tails) as after a −30 mV prepulse (Fig. 3*C*, control tails, same neuron) suggesting that a noninactivating conductance underlies the fast tails. These data indicate that the fast tails represent the closing of the TEA-sensitive noninactivating conductance shown in Figures 1 and 2. Also consistent with this, the fast tails after −30 mV prepulses were completely blocked by 3 mM TEA (Fig. 3*C*).

←

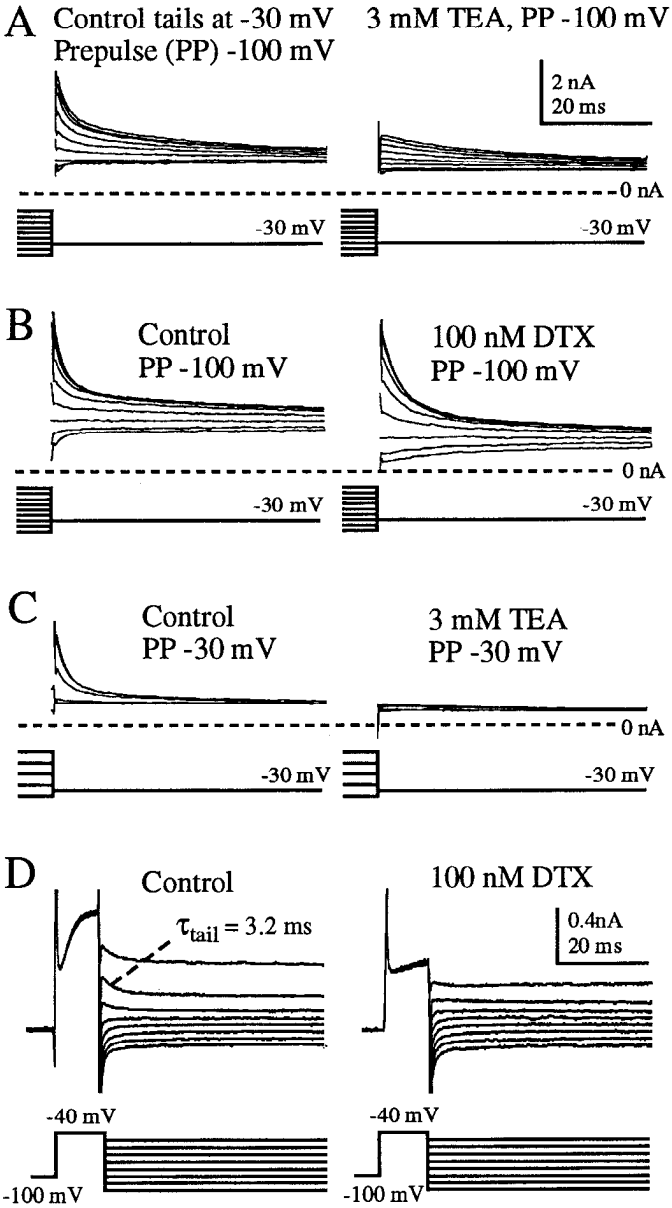

Figure 3. Tail currents indicate rapid closing of the TEA-sensitive conductance and I_d. *A*, The tail currents at −30 mV (after 180 msec at voltages of −50mV to +30 mV, following a 1 sec prepulse at −100 mV). The control tails after voltage steps positive to −10 mV included a large rapidly decaying component that was selectively blocked by 3 mM TEA. The slower component of the tails was unchanged. *B*, Tail currents from another MNTB neuron (same voltage protocol as *A*). The fast tail component was unaffected by 100 nM DTX. The slower tails were unchanged except for a slight reduction in the currents following the most negative voltage steps, as might be expected if only I_d was blocked. *C*, Tail currents from the neuron of *A*, using a similar protocol, but with a 1 sec inactivating prepulse at −30 mV before voltage steps between −40 mV and +40 mV. The rapidly decaying tail currents were blocked by 3 mM TEA. A slower component of the control tails was much smaller than in *A*. *D*, Rapidly decaying tail currents at potentials between −50 mV and −120mV represented the closing of I_d (note different current scale than for *A–C*). After a 500 msec prepulse at −100 mV, I_d opened to its maximum amplitude during a 10 msec step to −40 mV, in control ACSF-V. Tail currents that decayed rapidly with a single exponential time course were seen at −50 mV, −60 mV, and −70 mV. At −50 mV and −60 mV some steady outward current remained, consistent with partial closing of I_d at these potentials. In the presence of 100 nM DTX most of the I_d current during the 10 msec step to −40 mV was blocked, and the fast tail currents were much reduced.

Very positive voltage steps of shorter duration, lasting 3 msec instead of 180 msec, were followed by fast tails of similar or slightly increased magnitude (data not shown). This indicates that the TEA-sensitive, DTX-insensitive conductance opens rapidly at positive potentials (in less than 3 msec). The results of Figure 3*A–C* suggest that this conductance closes rapidly at −30 mV (t = 2 msec) and does not inactivate during one second at −30 mV (though it may show slight inactivation at more positive potentials).

I_d *also has rapid activation and deactivation kinetics*

After a 10 msec step to −40 mV, to open I_d, stepping down to more negative potentials caused I_d to close (or partly close) with rapid kinetics (Fig. 3*D*, control data). These tail currents decayed rapidly with a single exponential time course ($\tau tail$ = 2.9 ± 0.4 msec at −60 mV, n = 10). The tail currents were still outward at −70 mV, supporting the idea that the underlying conductance is selective for potassium ions. The current at −40 mV, and the subsequent tail currents, were mostly blocked by 100 nM DTX (Fig. 3*D*). Figure 1 showed that I_d activates rapidly at −30 mV or more positive. The data of Figure 3*D* show that the deactivation of I_d is also rapid.

The inactivation of I_d

The inactivation of I_d was investigated by subtracting DTX-insensitive currents from the control currents during a 19 sec voltage step to −30 mV (after a 500 msec step to −100 mV). The DTX-insensitive current that remained when 10 or 100 nM DTX were present activated very slowly (peaking at about 200 msec) and then inactivated slowly. The mean amount of current blocked by 10 or 100 nM DTX at −30 mV was 0.39 nA at 10 msec, 0.17 nA at 500 msec and 0.14 nA at 19 sec (n = 4). Thus, the DTX-sensitive current was 56% inactivated within 500 msec, and inactivated by only a further 7% in the next 18.5 sec (n = 4). The exact timecourse of the partial inactivation of I_d was not clearly distinguishable, partly because the kinetics of the slowly activating DTX-insensitive current influenced the time course of the subtracted current records. Partial inactivation has been reported for currents similar to I_d in other neurons (e.g., Stansfeld et al., 1986) and potassium channels formed from cloned DTX-sensitive subunits (Hopkins et al., 1994a).

After 5 sec at −30 mV, I_d was partially inactivated and remained partially inactivated at −50 mV, but recovered from this inactivation during 500 msec at −100 mV, or more negative (Fig. 4*A*, currents measured at −40 mV). The inactivation curve for I_d was fitted using a Boltzmann function, with a voltage for half-inactivation (V_{half}) of −71.5 mV, and a K value of −8.4 mV for the neuron of Figure 4*B*. The mean V_{half} for inactivation was −69.2 ± 1.4 mV, with a K of −7.6 ± 0.7 mV (n = 21). (These mean values included fits from an alternative protocol, where 500 msec steps to −120 mV preceded the 500 msec inactivating steps, giving very similar results.) After including the −7 mV junction potential at the pipette tip, the mean V_{half} for inactivation would be −76 mV.

In order to check that the partial inactivation of I_d had not led us to estimate V_{half} wrongly, we fitted alternative inactivation curves that assumed I_d could achieve full inactivation. We used the extrapolated leak current at −40 mV as a maximum estimate of the hypothetical fully inactivated level of I_d (the dotted line in Fig. 4*A*) and fitted a curve through this point and the previous inactivation data (including only the current values after inactivating pulses of −60 mV or more negative, which resulted in

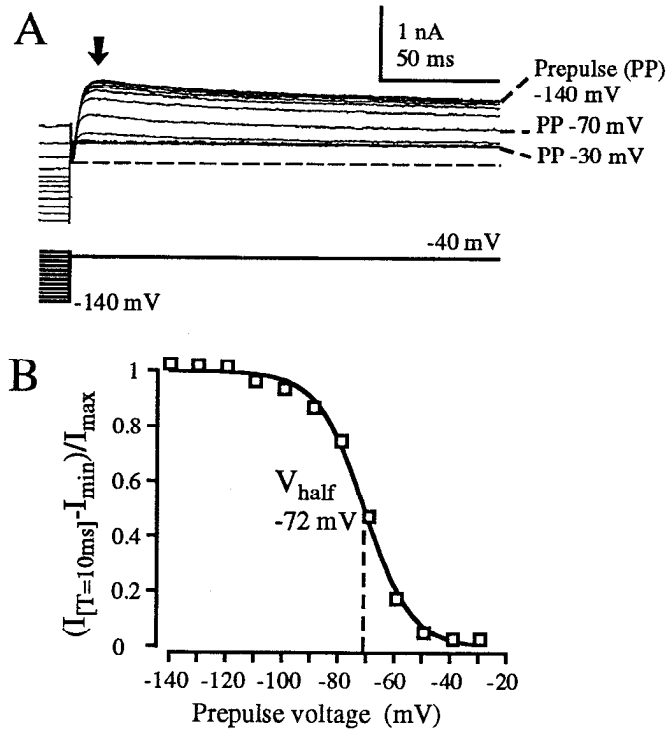

Figure 4. The voltage dependence of inactivation of I_d. *A*, The inactivation of I_d currents. An MNTB neuron was held at −30 mV for 5 sec, and then stepped to prepulse potentials between −140 mV and −30 mV for 500 msec before returning to a test potential of −40 mV (at which potential I_d is the predominant current). Inactivation of I_d depended on voltage, with −100 mV causing no inactivation. The *dotted line* is the extrapolated leak current at −40 mV, using the −70 mV to −100 mV prepulse current levels. *B*, The voltage dependence of inactivation of I_d calculated using the current values at the time shown by the *solid arrow* in *A* (measured 10 msec after the start of steps to −40 mV) to construct an inactivation curve (*open squares*). A Boltzmann equation was fitted to the data (including variables for fitting the maximum and minimum current levels). The voltage at which half the current was inactivated was −71.5 mV and *K* was −8.4 mV. In this protocol there was only partial inactivation of the I_d conductance (see Results).

equilibrium levels of inactivation). This gave a mean V_{half} of −64.0 mV (K −10.2 mV, n = 10) or −71 mV after including the junction potential. The true value for V_{half} is likely to be somewhere between these −71 mV and −76 mV values. Thus, an MNTB neuron has over half of its I_d channels inactivated at −70 mV, which is the resting membrane potential of MNTB neurons (Forsythe and Barnes-Davies, 1993a).

I_d recovered rapidly from inactivation. After a prolonged inactivating step to −30mV, steps to −120 mV for as little as 5 msec could produce some recovery from inactivation, whereas an 100 msec step produced complete recovery. The time course of recovery from inactivation was approximately fitted by a single exponential, with a mean time constant of 31.3 ± 5.7 msec (n = 7, data not shown).

Other voltage-dependent potassium conductances in MNTB neurons

The time course of the more slowly decaying current tail component in Figure 3, *A* and *B* (τ = 24.5 ± 4.3 msec, n = 11), probably reflects channel inactivation, as well as partial closing of channels to their −30 mV equilibrium level. The reduction or abolition of the slow component after one second at −30 mV (Fig. 3*C*) suggests that an inactivating conductance, or conductances, underlies the slow decay. Most of the slowly decaying component was not blocked by 100 nM DTX, suggesting that MNTB neurons possess a third conductance type that inactivates and is DTX-insensitive (Fig. 3*B*). All three of these MNTB neuron potassium conductances were sensitive to micromolar concentrations of 4-aminopyridine (4-AP) (data not shown).

The low [Ca^{2+}] (and raised [Mg^{2+}]) in the control ACSF-V minimized any currents flowing through calcium channels or Ca^{2+}-activated potassium channels ($I_{K(Ca)}$) in MNTB neurons. The MNTB neuron potassium currents seen in an ACSF containing 2 mM [Ca^{2+}] (similar to ACSF-C except for the addition of tetrodotoxin and strychnine as in ACSF-V) looked very similar to those in ACSF-V and the application of 100 μM cadmium to block calcium channels had little effect. This suggests that very little of the outward current in MNTB neurons was $I_{K(Ca)}$ and that none of the three current components described was $I_{K(Ca)}$.

Dendrotoxin-I dramatically alters an MNTB neuron's response to depolarization

The activation ranges and rapid kinetics of I_d and the delayed rectifier conductance described above are relevant to their functional effects on AP firing in MNTB neurons. The complementary functional roles of these conductances are demonstrated by the following examination of the MNTB neurons under current clamp.

Depolarizing current-clamp steps produced a typical single AP response in MNTB neurons (in the ACSF-C for current clamp). A current step of +0.75 nA or more caused a single brief AP (2–5 msec after the start of the step) followed by a large afterhyperpolarization (AHP) that decayed into a plateau phase during which no further APs occurred (Fig. 5*A*). Some MNTB neurons produced two APs at the start of the largest current steps (data not shown) but there was never a graded response to increasing current as is typical of many CNS neurons. The current steps required to generate an AP were smaller than the typical mean peak amplitudes of EPSCs, over +3 nA, which are reached in less than 1 msec (Barnes-Davies and Forsythe, 1995). When current pulses 1 msec in duration were applied to MNTB neurons, the typical current magnitudes required to generate an AP were +3 nA or more, similar to EPSC amplitudes (data not shown) supporting the idea that the large size of the EPSP is essential to cause a short latency AP response.

The application of 100 nM DTX dramatically altered the MNTB neuron response to current steps, resulting in the generation of a train of APs (Fig. 5*B*). Each AP in the train was followed by a large AHP. For the largest current steps, of +1.5 nA, a high frequency AP train occurred (around 140 Hz) and there was no change in the duration or amplitude of the initial AP. In control ACSF-C, +0.75 nA steps gave initial APs of 0.8 msec duration (measured at −10 mV) and a mean peak amplitude of +44 mV (the mean values from three +0.75 nA steps for the neuron of Fig. 5*A–C*). In 100 nM DTX, the AP duration was 0.9 msec and the AP amplitude was +49 mV. Thus, DTX increased the number of APs in the response to current steps, with little effect on the size or shape of the initial AP or AHP.

The duration of APs was increased and the AHPs were abolished when 1 mM TEA was applied, in the presence of 100 nM DTX (Fig. 5*C*). The duration of the initial APs was increased to 1.5 msec and the AP amplitude increased to +61 mV. For each stimulus magnitude, the MNTB neuron produced a lower

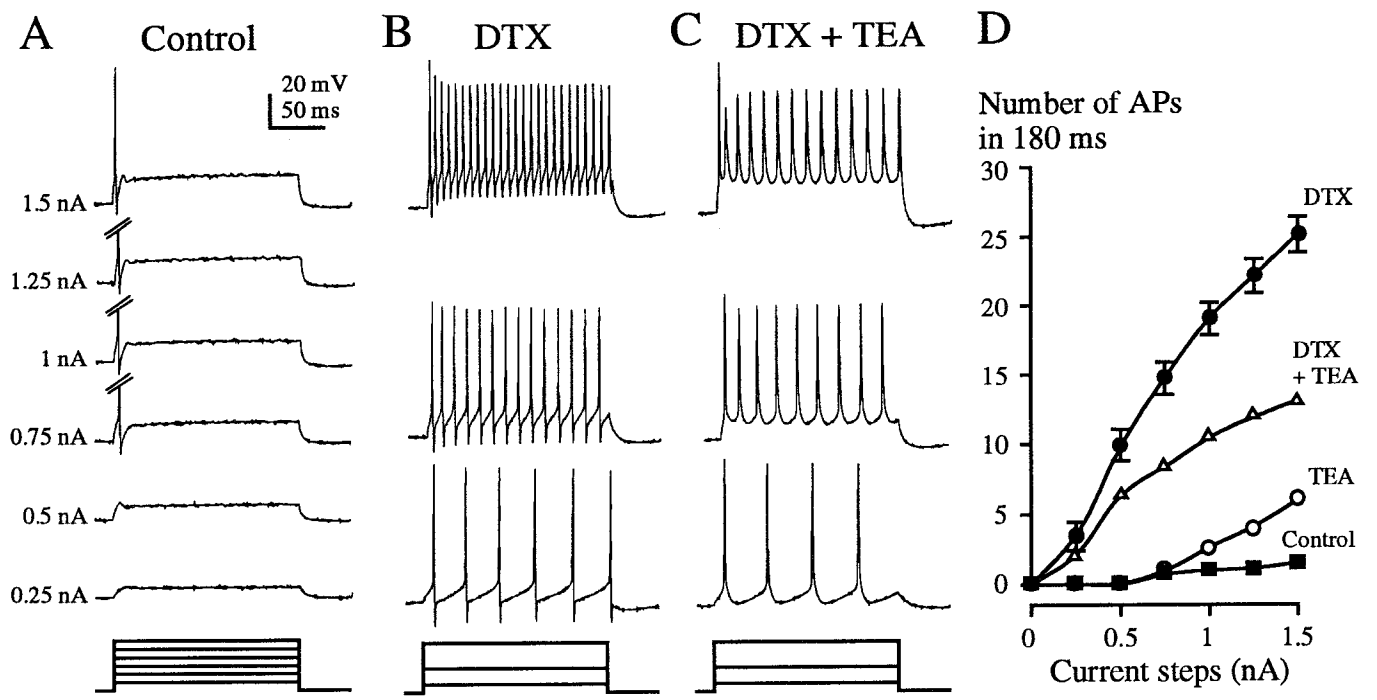

Figure 5. The effects of DTX and TEA on AP frequency and time course. The pipette resting potential was between −65 and −67mV for *A–C*. *A*, In control ACSF-C, the response of an MNTB neuron to depolarizing current-clamp steps was one action potential (*AP*) at the start of current steps greater than or equal to 0.75 nA (some of the APs are truncated to fit on the page). The AP was brief (less than 1 msec) and there was a large brief afterhyperpolarization (AHP). *B*, In 100 nM DTX, the MNTB neuron responded to a previously subthreshold stimulus (0.25 nA) with a train of APs. 1.5 nA produced a high frequency train of APs, but the duration of the AP and the size of the AHP were unaffected. *C*, In 100 nM DTX and 1 mM TEA, the MNTB neuron fired fewer APs than in DTX alone. The duration of APs increased and the AHPs disappeared. *D*, The dependence on current magnitude of the mean number of APs during 180 msec was altered by 100 nM DTX and/or 1 mM TEA (the modal numbers of APs at each current magnitude were measured for each neuron before calculating the mean). In control ACSF-C, the mean number of APs was between zero and 1.4 (n = 9 MNTB neurons). In 100 nM DTX, the mean number of APs was between zero and 25 (at 1.5 nA). The SE bars indicate the population variability in the current-clamp responses to DTX (n = 9 MNTB neurons). When 1 mM TEA was applied in the presence of 100 nM DTX, the largest depolarizing stimuli generated a reduced number of APs (n = 2). When 1 mM TEA was applied alone, only the largest current steps produced more than a single AP (n = 2).

frequency train of APs than in DTX alone. During the +1.5 nA steps, the reduced amplitude and increased duration of the second and subsequent APs was assumed to be related to increased levels of sodium channel inactivation (due to membrane depolarization and loss of the AHPs). We could not detect any consistent effect of either DTX or TEA on MNTB neuron resting membrane potentials.

Figure 5*D* is a graph showing the effects of DTX and TEA on the number of APs generated at different current step amplitudes. DTX reduced the threshold current required to generate APs, to 0.25 nA, which would have generated no APs under control conditions (n = 9). The addition of TEA in the presence of DTX hardly affected AP numbers for small current steps, but reduced the frequency of AP firing during the larger current steps. In contrast, the application of 1 mM TEA alone produced increased AP numbers, but only in response to large current steps.

Interpreting the current-clamp results in the light of the voltage-clamp data

The results of Figure 5 suggest that DTX blocks a potassium conductance that acts to limit the generation of APs during sustained depolarization (but is not essential for the brevity of each AP). The properties of the I_d conductance described above are suitable for this function. I_d channels open rapidly not far positive to rest, and then remain open, since their inactivation is slow. This is sufficient to keep the neuronal membrane just below AP firing threshold (−45 mV for initial APs, or more positive for mid train APs). It is particularly remarkable that such a small current can have such a dramatic AP limiting effect − the average I_d current at −47 mV was 0.36 nA (pipette potential −40 mV). Since the conductance is more than half inactivated at the MNTB neuron resting membrane potential of −70 mV, the I_d current would be less than 0.18 nA at −47 mV. The small size of I_d compared to the depolarizing currents it can oppose could also suggest a strategic location for the I_d channels at the axon hillock of MNTB neurons.

The data also suggest that 1 mM TEA blocked a potassium conductance that shortens the duration of APs by contributing to rapid AP repolarization and AHP generation. This is probably the TEA-sensitive delayed rectifier conductance described above. The high voltage activation threshold of this conductance could also explain the failure of 1 mM TEA alone to cause APs for the smallest current steps (Fig. 5*D*) during which the membrane potential remains too negative to activate this conductance.

The reduction in AP frequency when 1 mM TEA was applied in the presence of DTX (Fig. 5*B–D*) suggests that one function of rapid AP repolarization and AHP generation is to deinactivate sodium channels that have inactivated during an AP, so that the MNTB neuron can fire a second AP after a very short interval. The potassium conductance responsible would therefore be es-

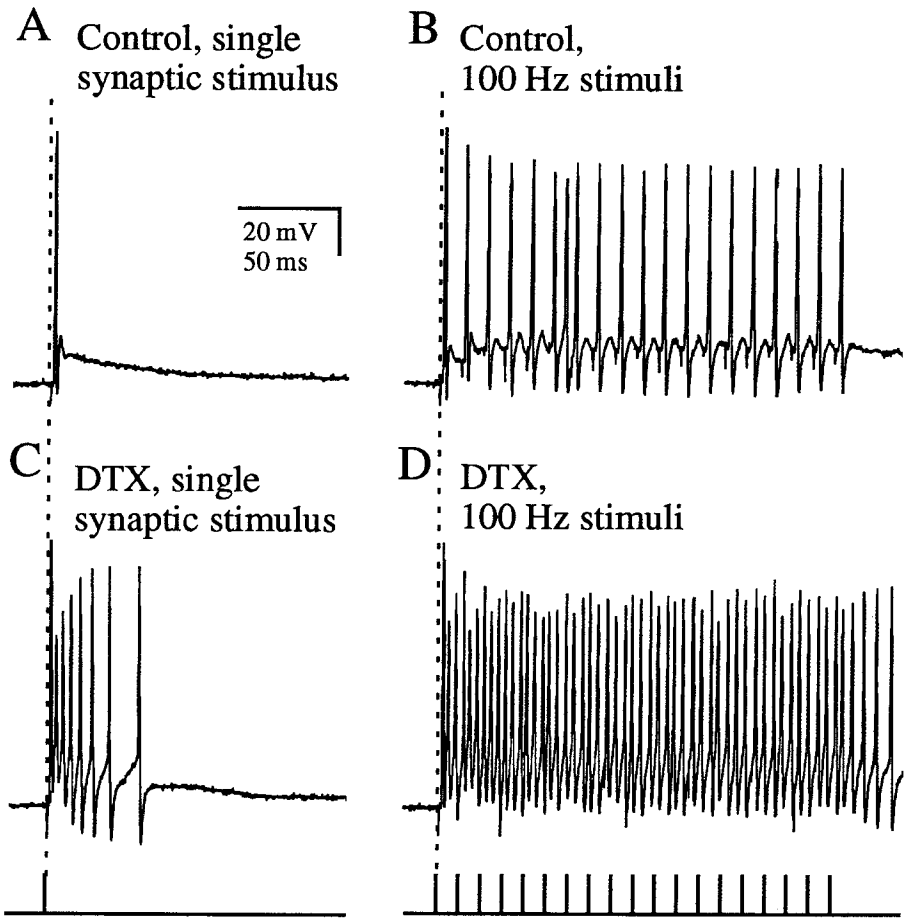

Figure 6. DTX increases the number of APs evoked by synaptic stimuli. The AP responses of a current-clamped MNTB neuron to synaptic stimulation. Axonal stimuli were applied at 2 sec intervals using a bipolar stimulating electrode that straddled the trapezoid body. The timing of axonal stimuli is shown by the bar at the bottom. The pipette resting potential was −69 mV, increasing to −74 mV in DTX. *A*, In control ACSF-C, the MNTB neuron generated a single AP in response to a single stimulation of its presynaptic axon. *B*, In control ACSF-C, a roughly phase-locked 100 Hz train of APs was generated in response to 100 Hz stimulation of the presynaptic axon for 200 msec. *C*, When 100 nM DTX was applied, several high frequency APs occurred as a result of the single stimulation. *D*, When 100 nM DTX was applied, several high frequency APs occurred for each stimulation of the 100 Hz train, resulting in APs firing at 200–300 Hz.

sential for high frequency neuronal firing, including the MNTB neurons' high frequency responses to their giant synapse. The TEA-sensitive delayed rectifier conductance in MNTB neurons has the fast kinetics suitable to underlie this rapid AP repolarization, AHP generation, and high frequency firing ability.

DTX degrades the temporal fidelity of synaptic transmission by blocking I_d

Block of the DTX-sensitive postsynaptic conductance dramatically increased AP firing during MNTB neurons' responses to giant synaptic stimulation (Figs. 6, 7) suggesting a dominant role for I_d in postsynaptic integration.

In MNTB neurons with a functional input synapse, a single stimulation of the presynaptic axon (in the trapezoid body) invariably caused a single giant EPSC (under voltage clamp; Fig. 7*A*, lower trace) or a single AP (under current clamp, Figs. 6*A*, 7*A*). In the presence of 100 nM DTX a single axonal stimulation produced several postsynaptic APs (Fig. 6*C* and top trace of 7*B*) but only a single giant EPSC (Fig. 7*B*, lower trace). Thus, DTX block of I_d allowed the MNTB neuron to generate extra APs during the EPSP tail, preventing it from faithfully reproducing the single presynaptic AP occurring in its calyx.

DTX also dramatically increased AP firing during the MNTB neuron response to 100 Hz stimulation. In control ACSF-C, a single postsynaptic AP was seen for each presynaptic stimulation of a 100 Hz train of 200 msec duration (Fig. 6*B* and Fig. 7*C*, top trace). MNTB neurons were also able to faithfully follow stimulation of their presynaptic axon at 200 Hz (data not shown). In 100 nM DTX, several APs occured for each presynaptic stimulation, resulting in a runaway 200–300 Hz response to 100 Hz stimulation (Fig. 6*D* and Fig. 7*D*, top trace). Similar results were seen in five MNTB neurons. Each presynaptic stimulus within a 100 Hz train generated a single EPSC in a voltage-clamped neuron whether in control ACSF-C or in the presence of 100 nM DTX (lower traces of Fig. 7, *C* and *D*, respectively). The extra APs during EPSP tails in DTX meant that the MNTB neuron no longer reproduced a particular firing frequency of presynaptic APs, that is, DTX caused a loss of the temporal fidelity of AP transmission across the calyceal synapse.

DTX did not increase the amplitude of the EPSC, as would be expected if there had been an increase in transmitter release, due to a presynaptic mechanism. One of the first reported effects of DTX was increased release of the transmitter acetylcholine (Harvey and Karlsson, 1982). This is often interpreted as being due to block of potassium channels in presynaptic terminals, increasing AP duration, calcium entry and thus transmitter release. If there was any DTX-induced change in the mean EPSC response, it was insignificant compared to the large variability in individual EPSCs observed both in control ACSF-C and in 100 nM DTX, which had amplitudes ranging from 1 nA to 7 nA (Fig. 7, lower traces). This large variability does not cause any failures of the postsynaptic AP response, which is always a single AP in control ACSF-C and two or more APs in DTX. The dramatic effect of DTX on postsynaptic firing must therefore be due to block of the postsynaptic current I_d, rather than increased presynaptic transmitter release, since there was no change in EPSC amplitude or duration. However, extra postsynaptic APs could theoretically increase transmitter release at the MNTB

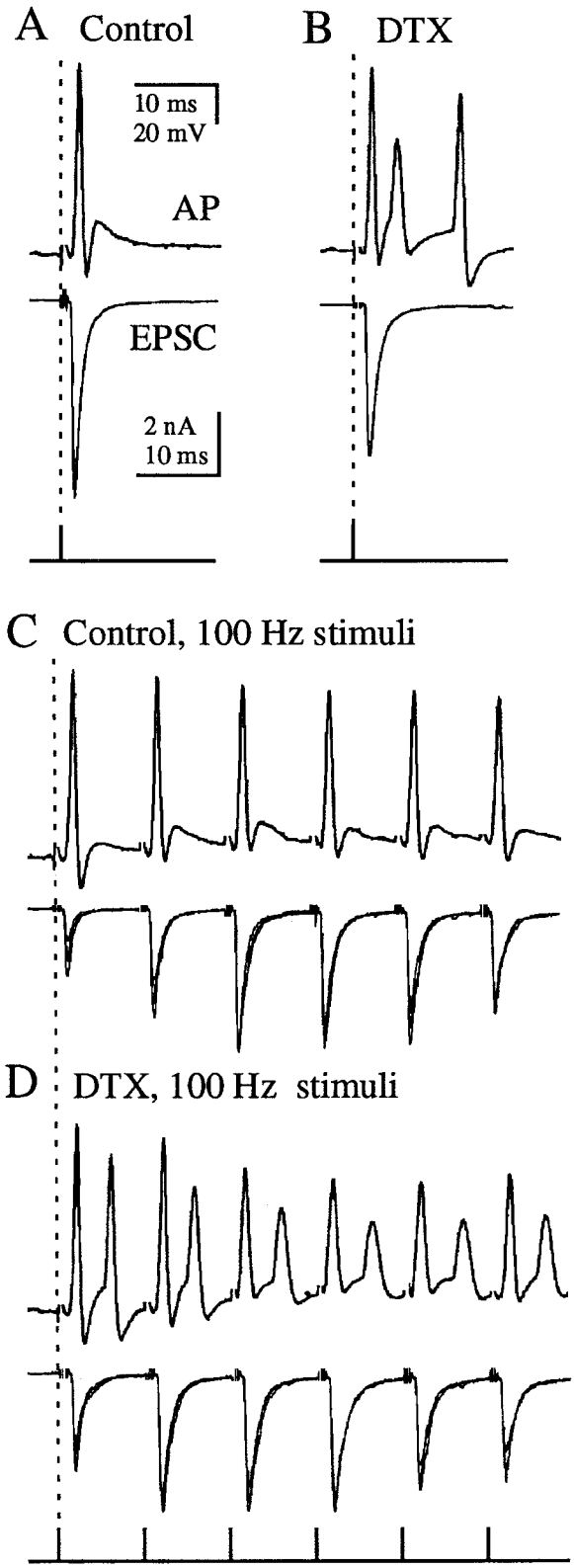

Figure 7. DTX affects postsynaptic APs but not giant EPSCs. An MNTB neuron was current clamped (*top traces*) or voltage clamped at −80 mV (*lower traces*) and series of 10 single or 100 Hz stimuli were applied at two second intervals. The pipette resting potential was −68 mV in control ACSF-C, decreasing to −64 mV in DTX. *A*, In control ACSF-C, a single axonal stimulus caused the MNTB neuron to generate a single AP riding on a giant EPSP, or a single giant EPSC. The average of 6 EPSCs is shown. (A slight synaptic depression developed during the first three of a series of single EPSC responses, which were therefore excluded from the averages). *B*, When 100 nM DTX was applied, several high frequency APs occurred as a result of the single stimulation. The mean time course of the EPSC (average of 6) was unaffected. *C*, In control ACSF-C, 100 Hz axonal stimulation generated an 100 Hz train of APs or a 100 Hz train of giant EPSCs. Three superimposed EPSC trains are shown (not including the first few applications of 100 Hz stimuli, during which the amplitude of the first EPSC in the train decreased, from about 6 nA to about 2 nA). The increasing amplitudes of the first few EPSCs in each train were presumed to be due to calcium accumulation inside the calyx. *D*, When 100 nM DTX was applied, more than one AP occurred for each stimulation of the 100 Hz train, resulting in APs firing at about 200 Hz. The giant EPSCs were unaffected.

neurons' output synapses. Thus, postsynaptic block of somatic I_d currents could explain the potentiation of transmitter release by DTX in other preparations.

Discussion

Our analysis of MNTB neuron potassium currents, APs and synaptic responses shows that a low voltage threshold conductance (I_d) suppresses multiple AP firing during the EPSP tail and another high voltage threshold conductance contributes to rapid AP repolarization and high frequency firing. Together they maintain the temporal fidelity of transmission across this giant synapse in the auditory pathway. These conductance types probably correspond to potassium channels including subunits from the *Shaw* and *Shaker*-related mammalian gene families, respectively (see below).

I_d, *single AP responses, and the giant synapse onto MNTB neurons*

Our results show that during small current steps, I_d channels open and prevent the MNTB neuron from reaching AP threshold. When larger currents generated a single AP, I_d channels were open following the AP, creating the silent plateau phase of the response by opposing depolarization sufficiently to prevent further APs.

A single synaptic stimulation also caused a single AP response (or a single giant EPSC). DTX caused several APs to be generated for each EPSP. This suggests that, under control conditions, I_d opposed depolarization during the tail end of the EPSP. DTX caused a dramatic loss of the temporal fidelity of transmission of APs across the giant synapse, by allowing multiple firing for each EPSP.

High frequency synaptic fidelity in the auditory system

AMPA receptors desensitize particularly rapidly in many auditory neurons (Raman et al., 1994; Barnes-Davies and Forsythe, 1995) and are thought to contribute to high frequency synaptic fidelity by causing a rapidly decaying EPSP. This paper suggests that open I_d channels facilitate fast EPSP decay by reducing the membrane time constant. The EPSCs include a slower NMDA-receptor mediated component, that might be expected to influence AP firing during high frequency stimulation, but does not do so in the chick equivalent of bushy neurons (Zhang and Trussell, 1994a) probably because an I_d-like current opposes depolarization between EPSPs.

MNTB neurons' high frequency temporal fidelity probably also depends critically on rapid AP repolarization and large AHPs. The resultant rapid recovery of sodium channels from inactivation, and brevity of the refractory period means that APs can be generated at nearly double the frequency than when the

←

TEA-sensitive conductance is blocked (Fig. 5). Thus, the presence of the AP-repolarising delayed rectifer conductance confers high frequency firing capability on the MNTB neuron, and is likely to be essential for high frequency following of presynaptic APs (>600 Hz at 37°C; Wu and Kelly, 1993).

Auditory frequency discrimination is partly based on tonotopic organization, but also utilizes phase-locked APs that can partially represent frequencies higher than maximal auditory neuron firing frequencies (Goldberg and Brown, 1969). An invariant latency of the postsynaptic AP response is crucial to preserve the precise relative timing of APs carrying phase-locked information. The fast delayed rectifier conductance could contribute to an invariant delay in responses during a high frequency EPSP train, by its rapid "resetting" of sodium channel responsiveness, and subsequent rapid closing. If I_d was not present, the extra APs generated during high frequency trains of EPSPs could degrade the timing precision of the initial AP response to each EPSP. Thus, both these conductances are likely to be crucial for the temporally faithful transmission of phase locked AP sequences.

I_d and DTX-sensitivity in other neuronal preparations

The first I_d described (4-AP-sensitive, low voltage threshold, slowly inactivating) in a fast-conducting subgroup of rat nodose ganglion sensory neurons, was blocked by 3–10 nM α-dendrotoxin (α-DTX) and also limited the AP response to depolarizing current, to one or two initial APs (Stansfeld et al., 1986). The fastest conducting subgroup of neurons in the rabbit nodose ganglion also followed vagal stimulation at the highest frequencies (Stansfeld and Wallis, 1985) suggesting that I_d was performing a similar function to that seen in MNTB neurons.

The Toxin-I (DTX-I, from black mamba venom) used here blocks neuronal potassium currents with slightly higher potency than α-DTX from green mamba (Halliwell et al., 1986; Brau et al., 1990; Hall et al., 1994). The I_d-like-current at frog nodes of Ranvier (Dubois, 1981) has an IC_{50} for current block of 0.4 nM for DTX-I (Benoit and Dubois, 1986) and 11 nM for α-DTX (Brau et al., 1990). In rat motor axons, 4-AP converted the single AP response to a brief stimulus to a short burst of impulses (Baker et al., 1987) perhaps reflecting block of an I_d-like current. Interestingly, the Kv1.1 and Kv1.2 potassium channel subunits that could underlie I_d currents in MNTB neurons (see below) are also present at mouse nodes of Ranvier (Wang et al., 1993) suggesting that these subunits or their amphibian analogues could underlie nodal I_d-like currents in frogs and mammals. α-DTX-sensitive single channel currents have been described in membrane patches from cultured dorsal root ganglion neurons (Stansfeld and Feltz, 1988) and frog nodes (Jonas et al., 1989).

In hippocampal slices, 300 nM α-DTX blocked 76% of a low threshold, transient neuronal potassium current (Halliwell et al., 1986). A low voltage threshold, slowly inactivating, 4-AP-sensitive and TEA-insensitive current (I_d) caused delays in AP firing in neurons in hippocampal slices (Storm, 1988) and the effect of 4-AP or 30 nM α-DTX on firing in neostriatal spiny neurons in slices suggested they possess a similar I_d (Nisenbaum et al., 1994).

I_d currents are small enough to have been overlooked in some neurons (see Figs. 1, 2). For example, a previous study from this laboratory stated that 1 μM DTX-I had little effect on MNTB neuron currents, since they were measured from a −60 mV holding potential which would have inactivated more than half of I_d (Forsythe and Barnes-Davies, 1993a). In the same study, the effect of 4-AP on MNTB neuron firing was very similar to the effect of TEA and DTX-I in Figure 5*C* of this article, presumably because 4-AP blocked both I_d and the high threshold TEA-sensitive conductance.

What potassium channel subunits form the MNTB conductances?

Sensitivity to dendrotoxin is confined to potassium channels including *Shaker*-related subunits, thought to account for most of the widespread α-DTX-binding in the mammalian nervous system (Rehm and Lazdunski, 1988; Pelchen-Matthews and Dolly, 1989; Rehm et al., 1989). *Shaker* subunits Kv1.1 and Kv1.2 are present in mouse MNTB neurons (Wang et al., 1994). Channels formed from expressed Kv1.1 or Kv1.2 subunits have high α-DTX-sensitivity (IC_{50} for current, 20 nM and 17 nM) and low voltage thresholds (Grissmer et al., 1994). Studies of heteromultimeric channels including both DTX-I-sensitive Kv1.1 and insensitive Kv1.3 subunits suggest that high sensitivity to DTX-I can be conferred on channels by the inclusion of only a single sensitive subunit (Hopkins et al., 1994b). Kv1.1 channels are highly sensitive to TEA (apparent K_d, 0.3 mM) while Kv1.2 channels are TEA-insensitive (Grissmer et al., 1994; Hopkins et al., 1994a). This suggests that Kv1.2 subunits could dominate the properties of the relatively TEA-insensitive I_d channels in MNTB neurons.

Rat MNTB neurons express the mRNA for the *Shaw*-related potassium channel subunits Kv3.1 and Kv3.3, but not Kv3.2 or Kv3.4 (Perney et al, 1992; Weiser et al., 1994). Channels formed from the splice variant Kv3.1b were dendrotoxin-insensitive and had high voltage thresholds, fast tail currents and a K_d for TEA block of 0.3 mM (Grissmer et al., 1994). These properties are similar to those we have described above for the delayed rectifier currents in MNTB neurons. Similar large noninactivating currents were produced by channels formed from the alternatively spliced subunit Kv3.1a, while Kv3.3a produced small slowly inactivating currents (Weiser et al., 1994). These data suggest that the TEA-sensitive conductance in MNTB neurons could include predominantly Kv3.1 subunits.

Similar currents and high frequency fidelity in other auditory neurons

In MNTB neurons, I_d contributes outward current rectification around the resting potential. Such membrane nonlinearity around rest is thought to aid high frequency responsiveness to giant synapses onto other auditory neurons, by allowing large, rapid onset responses that recover quickly when low resistance reduces the membrane time constant. Other auditory neurons that follow high frequencies of stimulation show similar rectification (guinea-pig inner hair cells; Kros and Crawford, 1990) and single AP responses (mouse bushy neurons, Oertel, 1985; chick bushy neuron equivalents, Reyes et al., 1994, and Zhang and Trussell, 1994a). A low voltage threshold 4-AP-sensitive current that probably included an I_d was well described in a subgroup of neurons dissociated from guinea-pig anteroventral CN (Manis and Marx, 1991). These presumed bushy neurons fired one or two initial APs during current steps and had outward currents similar to MNTB neuron currents, including fast tail currents, suggesting similar channels are present in the afferent pathways to the MNTB. This idea is supported by the observation that the potassium channel subunits in MNTB neurons are also present in large anteroventral CN neurons, probably bushy neurons

(*Shaker* Kv1.1 and Kv1.2, Wang et al., 1994; *Shaw* Kv3.1 and Kv3.3, Weiser et al., 1994).

General functions of I_d *currents*

Many of the recordings of I_d currents have been in fast conducting axons, or neurons that have such axons. This could reflect analogous requirements of axons and the MNTB relay synapse. Both systems require rapid and secure transmission of APs and use a large current source to ensure that this occurs. The opening of I_d prevents AP responses to the tail region of the primary stimulus (sodium current or giant EPSC) facilitating rapid membrane recovery by decreasing the time constant. I_d may therefore perform analogous functions in axons and at the MNTB relay synapse, facilitating rapid, secure and temporally faithful AP transmission.

Bushy neurons receive between about 5 and 50 synapses. Since I_d-like currents are present in these neurons, they could preserve and enhance any synchronized temporal information in several synaptic inputs, perhaps also preventing less synchronized activity from disrupting accurate phase-locking. I_d could also enhance temporally correlated activity across synapses in nonauditory neurons with many synaptic inputs.

References

Baker M, Bostock H, Grafe P, Martius P (1987) Function and distribution of three types of rectifying channel in rat spinal root myelinated axons. J Physiol (Lond) 383:45–67.

Barnes-Davies M, Forsythe ID (1995) Pre- and Post-synaptic glutamate receptors at a giant excitatory synapse in rat auditory brainstem slices. J Physiol (Lond) 488:387–406.

Benoit E, Dubois JM (1986) Toxin I from the snake *Dendroaspis polylepis polylepis*: a highly specific blocker of one type of potassium channel in myelinated nerve fibre. Brain Res 377:374–377.

Brau ME, Dreyer F, Jonas P, Repp H, Vogel W (1990) A K^+ channel in *Xenopus* nerve fibres selectively blocked by bee and snake toxins: binding and voltage-clamp experiments. J Physiol (Lond) 420:365–385.

Brew HM, Forsythe ID (1994a) Auditory neurones of the rat MNTB possess potassium conductances that aid high fidelity, high frequency synaptic transmission. J Physiol (Lond) 480P:109.

Brew HM, Forsythe ID (1994b) A dendrotoxin-I sensitive potassium conductance in auditory neurons of the rat MNTB. Soc Neurosci Abstr 20:1524.

Dubois JM (1981) Evidence for the existence of three types of potassium channels in the frog Ranvier node membrane. J Physiol (Lond) 318:297–316.

Edwards FA, Konnerth A, Sakmann B, Takahashi T (1989) A thin slice preparation for patch clamp recordings from neurones of the mammalian central nervous system. Pfluegers Arch 414:600–612.

Forsythe ID (1994) Direct patch recording from identified presynaptic terminals mediating glutamatergic EPSCs in the rat CNS, *in vitro*. J Physiol (Lond) 479:381–387.

Forsythe ID, Barnes-Davies, M (1993a) The binaural auditory pathway: membrane currents limiting multiple action potential generation in the rat medial nucleus of the trapezoid body. Proc R Soc Lond [Biol] 251:143–150.

Forsythe ID, Barnes-Davies M (1993b) The binaural auditory pathway: excitatory amino acid receptors mediate dual time course excitatory postsynaptic currents in the rat medial nucleus of the trapezoid body. Proc R Soc Lond [Biol] 251:151–157.

Forsythe ID, Barnes-Davies M, Brew HM (1995) The calyx of Held: a model for transmission at mammalian glutamatergic synapses. In: Excitatory amino acids and synaptic transmission, 2d ed (Wheal H, Thomson A, eds), in press. London: Academic.

Goldberg JM, Brown PB (1969) Response of binaural neurons of dog superior olivary complex to dichotic tonal stimuli: some physiological mechanisms of sound localisation. J Neurophysiol 32:613–636.

Grissmer S, Nguyen AN, Aiyar J, Hanson DC, Mather RJ, Gutman GA, Karmilowicz MJ, Auperin DD, Chandy KG (1994) Pharmacological characterisation of five cloned voltage-gated K^+ channels, types Kv1.1, 1.2, 1.3, 1.5, and 3.1, stably expressed in mammalian cell lines. Mol Pharmacol 45:1227–1234.

Hall H, Stow J, Sorensen R, Dolly JO, Owen D (1994) Blockade by dendrotoxin homologues of voltage-dependent K^+ currents in cultured sensory neurons from neonatal rats. Br J Pharmacol 113:959–967.

Halliwell JV, Othman IB, Pelchen-Matthews A, Dolly JO (1986) Central action of dendrotoxin: selective reduction of a transient K conductance in hippocampus and binding to localized acceptors. Proc Natl Acad Sci USA 83:493–497.

Harvey AL, Karlsson E (1982) Protease inhibitor homologues from mamba venoms: facilitation of acetylcholine release and interactions with prejunctional blocking toxins. Br J Pharmacol 77:153–161.

Held H (1893) Die centrale Gehorleitung. Arch Physiol Anat Abt 17: 201–248.

Hopkins WF, Allen ML, Houamed KM, Tempel BL (1994a) Properties of voltage-gated K^+ currents expressed in *Xenopus* oocytes by mKv1.1, mKv1.2 and their heteromultimers as revealed by mutagenesis of the dendrotoxin-binding site in mKv1.1. Pfluegers Arch 428: 382–390.

Hopkins WF, Demas V, Tempel BL (1994b) Both N- and C-terminal regions contribute to the assembly and functional expression of homo- and heteromultimeric voltage-gated K^+ channels. J Neurosci 14: 1385–1393.

Jonas P, Brau ME, Hermsteiner M, Vogel W (1989) Single-channel recording in myelinated nerve fibers reveals one type of Na channel but different K channels. Proc Natl Acad Sci USA 86:7238–7242.

Kros CJ, Crawford AC (1990) Potassium currents in inner hair cells isolated from the guinea-pig cochlea. J Physiol (Lond) 421:263–291.

Manis PB, Marx SO (1991) Outward currents in isolated ventral cochlear nucleus neurons. J Neurosci 11:2865–2880.

Masterton RB, Imig TJ (1984) Neural mechanisms for sound localisation. Annu Rev Physiol 46:275–287.

Moore MJ, Caspary DM (1983) Strychnine blocks binaural inhibition in lateral superior olivary neurons. J Neurosci 3:237–242.

Nisenbaum ES, Xu ZC, Wilson CJ (1994) Contribution of a slowly inactivating potassium current to the transition to firing of neostriatal spiny projection neurons. J Neurophysiol 71:1174–1189.

Oertel D (1985) Use of brain slices in the study of the auditory system: spatial and temporal summation of synaptic inputs in cells of the anteroventral coclear nucleus of the mouse. J Acoust Soc Am 78: 328–333.

Pelchen-Matthews A, Dolly JO (1989) Distribution in the rat central nervous system of acceptor subtypes for dendrotoxin, a potassium channel probe. Neuroscience 29:347–361.

Perney TM, Marshall J, Martin KA, Hockfield S, Kaczmarek LK (1992) Expression of the mRNAs for the Kv3.1 potassium channel gene in the adult and developing rat brain. J Neurophysiol 68:756–766.

Raman IM, Zhang S, Trussell LO (1994) Pathway-specific variants of AMPA receptors and their contribution to neuronal signalling. J Neurosci 14:4998–5010.

Rehm H, Lazdunski M (1988) Purification and subunit structure of a putative K^+-channel protein identified by its binding properties for dendrotoxin-I. Proc Natl Acad Sci USA 85:4919–4923.

Rehm H, Newitt RA, Tempel BL (1989) Immunological evidence for a relationship between the dendrotoxin-binding protein and the mammalian homologue of the *Drosophila Shaker* K^+ channel. FEBS Lett 249:224–228.

Reyes AD, Rubel EW, Spain WJ (1994) Membrane properties underlying the firing of neurons in the avian cochlear nucleus. J Neurosci 14:5352–5364.

Stansfeld CE, Feltz A (1988) Dendrotoxin-sensitive K^+ channels in dorsal root ganglion cells. Neurosci Lett 93:49–55.

Stansfeld CE, Wallis DI (1985) Properties of visceral primary afferent neurons in the nodose ganglion of the rabbit. J Neurophysiol 54:245–260.

Stansfeld CE, Marsh SJ, Halliwell JV, Brown DA (1986) 4-Aminopyridine and dendrotoxin induce repetitive firing in rat visceral sensory neurons by blocking a slowly inactivating outward current. Neurosci Lett 64:299–304.

Storm JF (1988) Temporal integration by a slowly inactivating K^+ current in hippocampal neurons. Nature 336:379–381.

Strydom DJ (1976) Snake venom toxins. Purification and properties of low molecular weight polypeptides of *Dendroaspis polylepis* (black mamba) venom. Eur J Biochem 69:169–176.

Tolbert LP, Morest DK, Yurgelun-Todd DA (1982) The neuronal architecture of the anteroventral cochlear nucleus of the cat in the region of the cochlear nerve root: horseradish-peroxidase labelling of identified cell types. Neuroscience 7:3031–3052.

Wang H, Kunkel DD, Martin TM, Schwartzkroin PA, Tempel BL (1993) Heteromultimeric K^+ channels in terminal and juxtaparanodal regions of neurons. Nature 365:75–79.

Wang H, Kunkel DD, Schwartzkroin PA, Tempel BL (1994) Localization of Kv1.1 and Kv1.2, two K^+ channel proteins, to synaptic terminals, somata, and dendrites in the mouse brain. J Neurosci 14: 4588–4599.

Weiser M, VegaSaenz de Miera E, Kentros C, Moreno H, Franzen L, Hillman D, Baker H, Rudy B (1994) Differential expression of *Shaw*-related K^+ channels in the rat central nervous system. J Neurosci 14:949–972.

Wenthold RJ, Huie D, Altschuler RA, Reeks KA (1987) Glycine immunoreactivity localized in the cochlear nucleus and superior olivary complex. Neuroscience 22:897–912.

Wu, SH, Kelly JB (1993) Response of neurons in the lateral superior olive and medial nucleus of the trapezoid body to repetitive stimulation: intracellular and extracellular recordings from mouse brain slice. Hearing Res 68:189–201.

Zhang S, Trussell LO (1994a) A characterization of excitatory postsynaptic potentials in the avian nucleus magnocellularis. J Neurophysiol 72:705–718.

Zhang S, Trussell LO (1994b) Voltage clamp analysis of excitatory synaptic transmission in the avian nucleus magnocellularis. J Physiol (Lond) 480:123–136.